Effects of Operating Conditions on Heat Removal from Polyethylene Reactors

Yan Jiang, Kim B. McAuley, and James C. C. Hsu
Dept. of Chemical Engineering, Queen's University, Kingston, Ontario, Canada K7L 3N6

A one-dimensional nonequilibrium model for multicomponent condensation is used to simulate a vertical single-pass shell-and-tube heat exchanger in an industrial gas-phase polyethylene reactor system. Starting the calculation at the top of the exchanger, the model can predict temperatures at the bottom of the exchanger within an accuracy of ± 5 *K as compared to three sets of industrial data. Sensitivities of model predictions were analyzed, including uncertainties associated with physical and transport property estimates, step size, and convergence criterion. Model predictions are not particularly sensitive to the estimation errors of physical and transport properties if K values are calculated using an equation of state applicable to both liquid and vapor phases. Effects of operating conditions on heat removal from polyethylene reactors were investigated for an existing process. It was quantitatively demonstrated why and how severely noncondensable gases impede condensation heat transfer. The level of noncondensable gases and the cooling water temperature are the two most important factors influencing the heat-removal rate. Replacing a portion of noncondensable gas, such as* N_2*, with a condensable fluid that is inert to polymerization reactions can substantially increase the heat-removal rate from the reactor, thereby allowing for an increase in polymer production rate.*

Introduction

For gas-phase fluidized-bed polethylene reactors, heat removal from the reaction zone is one of the controlling factors that limits the production rate (Jenkins et al., 1986). The most common means of heat removal is to compress and cool the recycle gas mixture in an external heat exchanger. The recycle gas is then combined with fresh feed to the reactor. An industrial gas-phase polyethyelene reactor system is shown in Figure 1. Because the recycle stream is much larger than the fresh feed due to low conversion per pass (2–5%) (Choi and Ray, 1985), the cooling capacity of the recycle gas is a dominant factor that determines the maximum possible production rate of polymer. Substantial increases in space–time yields have been achieved by introducing condensed mode operation (Burdett, 1988). In condensed mode operation, a portion of the recycle-gas mixture is condensed in the heat exchanger and the resulting liquid/vapor mixture is then returned to the reactor. As a result, the cooling capacity of the recycle stream is increased due both to the lower temperature of the entering recycle stream, and the latent heat of vaporization of condensed liquid entrained in the recycle stream. It has been shown that the heat-removal rate can be further increased by adding nonpolymerizing condensable materials to raise the dew point (Jenkins et al., 1986). For a safe reactor operation, however, the gas-to-liquid ratio should be maintained at a level sufficient to keep the liquid phase of the two-phase flow in an entrained or suspended condition. Jenkins et al. (1986) recommended that the level of liquid in the recycle stream be between 2 and 12 wt. % and not exceed 20 wt. %. The questions of how to optimize the space–time yield using condensed mode operation, and what is the upper limit of the liquid level in the fluidizing medium, have not been answered. Recently, DeChellis and Griffin (1994) developed a method for maintaining stable reactor operation and fluidization by monitoring both the bulk density of the poly-

Current address of Yan Jiang: Gas Phase Research and Development, NOVA Research and Technology Corporation, 2928–16th Street N.E., Calgary, Alta., Canada T2E 7K7.

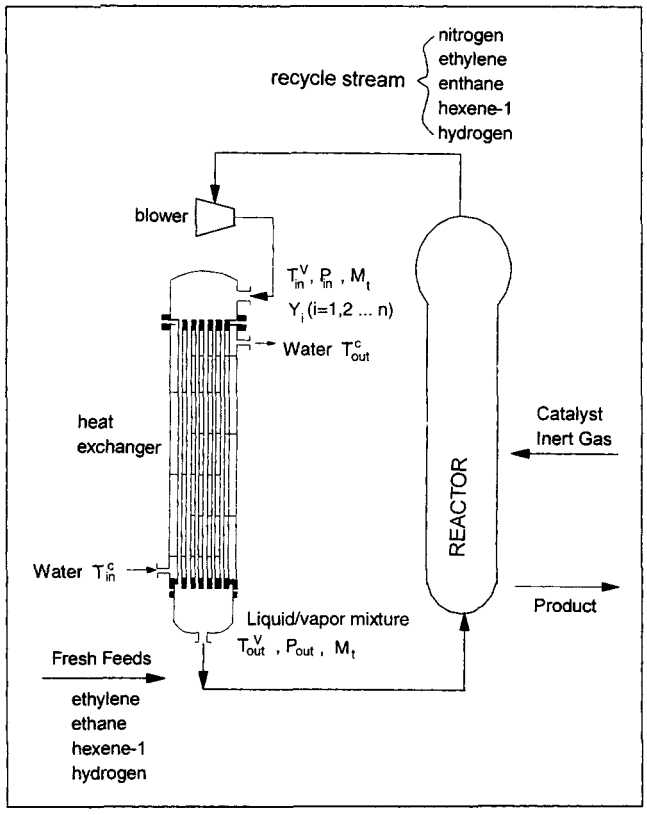

Figure 1. Industrial gas-phase polyethylene reactor system.

mer and the recycle gas density, and controlling the composition of the recycle stream to maintain desirable fluidization. As long as this monitoring is being done, DeChellis et al. (1995) suggested that a much higher level of condensation be permitted in the fluidized medium. The level of condensation in the recycle stream can be as high as 50 wt. %.

However, very little is known about how to operate the process to obtain the maximum heat removal from the reactor. There is a lack of quantitative information about the extent that noncondensable gases impede condensation heat transfer. Our goal is to maximize the heat-removal rate from polyethylene reactors, thus leading to a maximum production rate. Developing a mathematical model that describes the multicomponent condensation process of the recycle stream in the heat exchanger will help improve understanding of heat-removal phenomena involved in the system, and may lead to further improvements in production rate. The objectives of the current article are to employ the one-dimensional nonequilibrium model described by Jiang et al. (1997) to simulate multicomponent condensation in a vertical heat exchanger in a polyethylene reactor system; to analyze the sensitivities of model predictions to uncertainties associated with physical and transport property estimations; and to investigate the effects of operating conditions of the heat exchanger and reactor system on the heat-removal rate from polyethylene reactors.

Model Equations

In a previous article (Jiang et al., 1997), we employed nonequilibrium methods based on film theory for modeling a vertical single-pass shell-and-tube heat exchanger in an industrial polyethylene reactor system. A detailed description of the model development can be found in that article. Only a list of the model equations and a brief description are given here.

Consider a multicomponent vapor mixture condensing inside a vertical tube. The vapor enters at the top of the tube with cooling water flowing countercurrent on the shell side. The differential material balance for each species of the mixture is

$$\frac{dV_i}{dA} = -N_i = -\frac{dL_i}{dA} \qquad i = 1, 2, \ldots, n, \tag{1}$$

where V_i and L_i are molar flow rates of component i in the vapor and liquid phases, respectively, and N_i is molar flux of component i. For the case of all components condensable (no component is completely noncondensable), the molar flux (N) can be calculated by Eq. 2:

$$(N) = [\,k^V][\Xi](y^V - y^I) + N_t(y^V), \tag{2}$$

where the total molar flux $N_t = \Sigma N_i$; $[\,k^V]$ is a matrix of zero-flux mass-transfer coefficients; and $[\Xi]$ is a matrix of correction factors to account for the high flux of mass transfer. Energy-balance equations can be derived for both the vapor flow and coolant flow, at the liquid/vapor interface, and at the tube wall, respectively. All energy balance equations are summarized in Table 1. In Eqs. 3 and 4, q^V is the conductive heat flux out of the bulk vapor phase. In Eqs. 4 to 6, h_o is an overall heat-transfer coefficient accounting for the resistances to heat transfer in the condensate liquid, in the tube wall, and in the coolant; h_L is the heat transfer coefficient in the condensate liquid; and h_{Wc} is the heat transfer coefficient accounting for the heat transfer resistances in the tube wall and in the coolant. Detailed discussions about methods for calculating matrix $[\,k^V]$ and $[\Xi]$, heat flux q^V, and heat-transfer coefficients h_L are given by Jiang et al. (1997). The model equations are completed by the following four assumptions:

1. The liquid phase is completely mixed with regard to composition. In this case, the following relation exists for the composition in the interface and in the bulk liquid phase from a material balance along the flow path:

Table 1. Energy Balance Equations

Energy balance for the vapor phase $m_V c_P^V \frac{dT^V}{dA} = -q^V.$	(3)
Energy balance at the liquid/vapor interface $h_o(T^I - T^c) = q^V + \sum N_i^L c_{Pi}^V (T^V - T^I) + \sum N_i^L \Delta h_i.$	(4)
Energy balance at the wall $h_L(T^I - T^W) = h_{Wc}(T^W - T^c).$	(5)
Energy balance for the coolant $m_c c_P^c \frac{dT^c}{dA_{outs}} = -h_{Wc}(T^W - T^c).$	(6)

$$x_i^I = x_i^L = L_i/\Sigma L_j. \tag{7}$$

2. Equilibrium between liquid and vapor phases at the interface is assumed, so that

$$y_i^I = K_i x_i^I \qquad i = 1, 2, \ldots, n. \tag{8}$$

3. The pressure is assumed constant throughout the heat exchanger.

4. The bulk temperature in the liquid phase is approximated by $T^L = (T^I + T^W)/2$.

A numerical method for solving the model equations is described by Jiang et al. (1997).

Comparison with Industrial Data

As described by Jiang et al. (1997), three correlation methods were used for estimating h_L, the heat transfer coefficient in the condensate film layer. It was found that Butterworth's (1983) method for shear-stress-controlled condensate flow gave the best agreement between the simulation results and industrial data. To have a more comprehensive look at the model predictions and their sensitivity to model and operating parameters, three sets of operating data obtained from an industrial reactor for gas-phase copolymerization of ethylene/butene and ethylene/hexene, respectively, and ethylene homopolymer, are compared with computer simulations. Butterworth's (1983) method for shear-stress-controlled condensate flow is utilized to estimate h_L in these simulations. As shown in Figure 1, the available industrial data include the temperature T_{in}^V, pressure P_{in}, flow rate M_t and composition of the entering recycle stream, and the temperature T_{out}^c of the cooling water stream exiting at the top of the exchanger. The temperatures (T_{out}^V and T_{in}^c) of the vapor stream exiting and cooling water stream entering at the bottom of the exchanger, are also measured. Simulations start at the top of the exchanger. The predicted temperatures at the bottom of the exchanger are compared with industrial data, which unfortunately are the only available industrial measurements. Figures 2, 3 and 4 show that the predicted outlet vapor phase temperature T_{out}^V and inlet cooling water temperature T_{in}^c are close to the industrial data, within about ± 5 K for an approximate 50 K difference of inlet gas temperature, T_{in}^V and outlet vapor-phase temperature, T_{out}^V. The difference between the calculated and measured temperatures at the bottom of the exchanger is likely due to an inaccurate estimation in K-values, or heat-transfer coefficients, or both.

At the point where condensation begins, the wall temperature T^W suddenly increases. One possible explanation is that the heat-transfer coefficient between the liquid and wall is much higher than the value between the gas and wall, which results in an abrupt increase of T^W. Physically, condensation is expected as soon as the wall temperature is below the dew

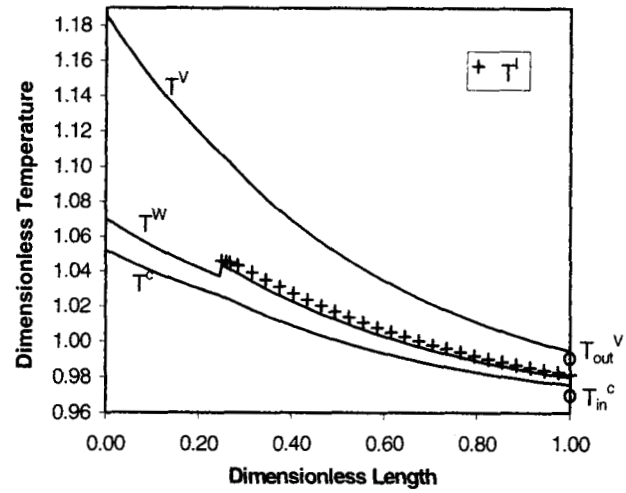

Figure 3. Temperature as a function of the length of the exchanger—comparing simulation results with industrial data for polymerizing ethylene alone, (○) industrial data at the bottom of the exchanger.

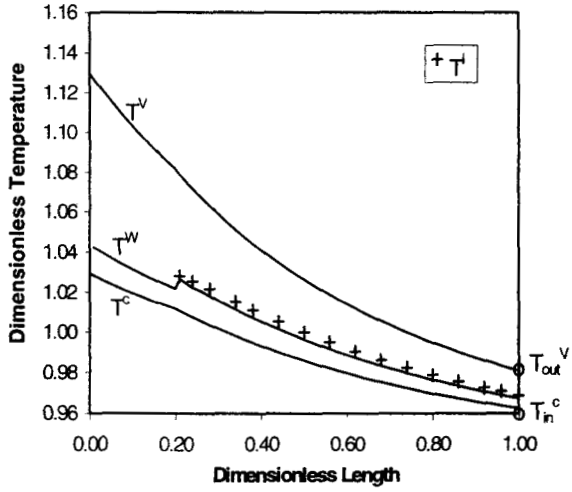

Figure 2. Temperature as a function of the length of the exchanger—comparing simulation results with industrial data for copolymerizing ethylene-butene, (○) industrial data at the bottom of the exchanger.

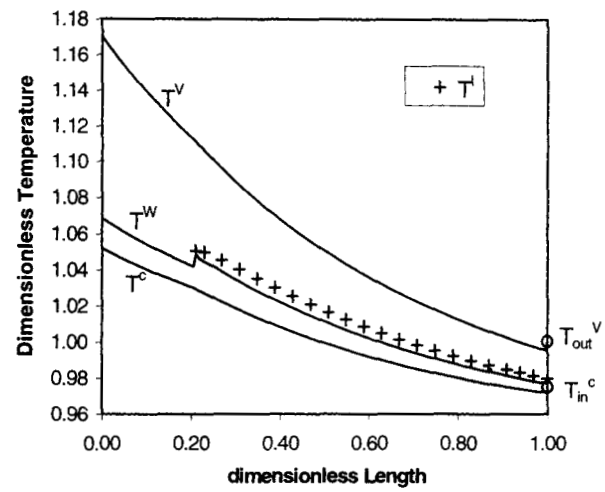

Figure 4. Temperature as a function of the length of the exchanger—comparing simulation results with industrial data for copolymerizing ethylene-hexene, (○) industrial data at the bottom of the exchanger.

point. In Figures 2–4, however, there exists a region in which the calculated wall temperatures are below the dew point, but the calculation assumes no condensation. It is likely because Butterworth's (1983) method is not appropriate for calculating h^L at the beginning of condensation, since initially the tube is not completely wetted. Since initially only a tiny amount of condensed liquid is present, high vapor shear stress may result in high liquid entrainment, or breakdown of the continuous liquid film. As suggested by Rosson and Meyers (1965), the methods for calculating h^L in the first period of condensation should be different from in the remaining part. Unfortunately, a better correlation for calculating h^L was not found in this work.

It should be noted that the initial interfacial temperatures (T^I) in these three systems are all about 5 K lower than the dew-point temperatures corresponding to their entering vapor compositions. Since the pressure is assumed constant throughout the heat exchanger, it cannot account for the difference. The reason for the difference is that the compositions at the liquid/vapor interface are different from those in the bulk vapor phase. This phenomenon can be illustrated using the computational results for the case of copolymerizing ethylene and butene in Figure 5. The composition profiles of three components are depicted in Figure 5, where the cross symbols represent the mole fraction, Y^I, at the liquid/vapor interface, and the solid curves represent the mole fraction, Y^V, in the bulk vapor phase. It can be seen that butene and isohexane compositions at the interface are lower than those in the bulk vapor phase; however, the noncondensable nitrogen mole fraction at the interface is higher than in the bulk vapor phase. In general, heavier (or less volatile) components have smaller diffusivities with respect to the mixture, while at the same time they have higher flux to the liquid–vapor interface than lighter (or more volatile) components. As heavier components move toward the interface, lighter components are swept to the interface as well by the fluxes of the heavier components. A dynamic equilibrium is set up, with relatively lighter or noncondensable gases accumulated at the liquid/vapor interface and less heavy or condensable components near the interface, resulting in the interface temperature, T^I, being lower than the bulk vapor-phase temperature, T^V. This temperature difference ($T^V - T^I$) creates a heat-transfer resistance in the liquid/vapor boundary layer. In turn, condensable components have to diffuse through noncondensable gases under the influence of their concentration gradients. Furthermore, Figure 5 shows that the difference ($Y^V - Y^I$) between the bulk vapor-phase mole fraction and the interfacial mole fraction for isohexane is larger than the value for butene. Hence, the simulation results demonstrate that the condensation driving force for isohexane is larger than the condensation driving force for butene, which is why more isohexane is condensed in the liquid phase.

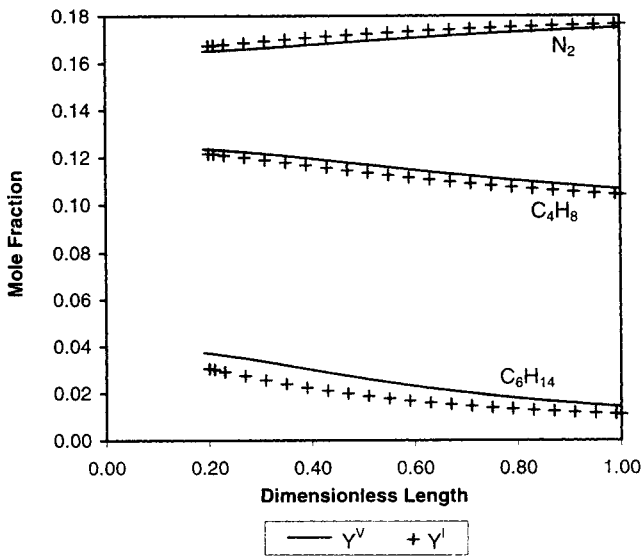

Figure 5. Mole fraction of several components as a function of the length of the exchanger.

Overall, starting the calculation from the top of the exchanger, the computation results obtained in this work can predict the temperatures at the bottom of the exchanger within an accuracy of about ±5 K for an approximate 50 K difference of ($T^V_{in} - T^V_{out}$). Reasonable results are also obtained for calculating the starting dew-point temperature and composition profiles in the vapor phase.

Model Sensitivity Analysis

Model sensitivities to the uncertainties in physical and transport property estimations

The steady-state model developed by Jiang et al. (1997) involves extensive physical and transport properties. However, there is little guidance in the literature concerning the uncertainties associated with physical and transport property estimates. Although the physical property estimation methods used here are the most appropriate methods among the available techniques described by Reid et al. (1987), it is important to analyze the sensitivity of the model predictions to the uncertainities related to physical and transport property estimates, so that one can understand the factors that affect model predictions. The physical and transport properties explicitly appearing in the model equations include heat capacity, c_P^V, in the vapor phase, K values, and partial molar enthalpies of vaporization, Δh_i. All the other physical and transport properties are used to estimate heat and mass-transfer coefficients, and therefore are implicit. The effect of the errors in physical and transport property estimates on the model predictions can be evaluated by looking at the changes of the major quantities that determine the performance of the heat exchanger, such as the heat-removal rate, the temperature drop, and the level of condensation.

Detailed descriptions of estimation methods for different physical and transport properties were given by Jiang (1997). Some of physical and transport properties are listed in Table 2, along with their corresponding expected prediction errors (Reid et al., 1987) and the uncertainties employed in sensitivity analyses for both the liquid and vapor phases. Since the two transport properties—heat capacity and diffusion coefficient—are only used in the model for vapor-phase calculations, corresponding prediction errors and uncertainties in the liquid phase are not required. A base case was chosen to perform sensitivity analysis according to the typical operating conditions of the heat exchanger and reactor system in industry. The specification of conditions at the top of the heat

Table 2. Expected Estimation Errors in Predicted Physical and Transport Properties

Physical or Transport Property		Density	Thermal Conduct.	Vis.	Heat Capacity	Diff. Coeff.
Vapor phase	Expected errors		5–8%	8–9%		4%
	Uncertainties chosen in sensitivity analysis	±3%	±8%	±9%	±3%	±4%
Liquid phase	Expected errors		5%	10–15%		
	Uncertainties chosen in sensitivity analysis	±5%	±15%	±15%		

exchanger for this base case is shown in Table 3, which, in fact, is used throughout this article for all sensitivity analysis and investigation of the effects of operating conditions on heat removal. The results for the three major quantities of interest were obtained for this base case as shown in Table 4. For each property, its lower and upper limits in the uncertainty range were used, keeping all the other property estimation methods unchanged to get a set of major quantities, which were then compared to those of the base case. Thus, only individual effects of the property estimation uncertainties have been analyzed. It can be seen from Table 4 that the model predictions are more sensitive to the property estimation errors in the vapor phase than in the liquid phase, probably because both mass- and heat-transfer calculations are performed in the vapor phase, while only heat-transfer calculations are important in the liquid phase. Comparing the three predicted quantities, the temperature drop is the least affected, while the total condensation rate is the most affected. The maximum uncertainty was found to be 2.28% when predicting the level of condensation, caused by the uncertainties of viscosity in the vapor phase. Larger uncertainties of the model predictions could result from combinations of errors in the physical properties. The effects of physical property prediction errors on individual component condensation rates are very small and are not shown in Table 4. In summary, the simulation results have indicated that the model predictions are not particularly sensitive to uncertainty in individual estimates of density, thermal conductivity, viscosity, heat capacity, or diffusion coefficients.

Table 3. Specification of Conditions at the Top of the Heat Exchanger for Base Case

Mole fraction of each component	2-Methylpentane	0.036801
	Isopentane	0.006394
	n-Butene	0.121930
	Ethane	0.042039
	Ethylene	0.346206
	Nitrogen	0.162852
	Methane	0.021302
	Hydrogen	0.262476
Entering dimensionless temperature of the recycle gas mixture	T_{in}^{V}	1.130
Total flow rate of the recycle gas mixture	kg/s per tube	0.1682
Exiting dimensionless cooling-water temperature	T_{out}^{c}	1.029
Coolant flow rate	kg/s	0.340
Pressure in the heat exchanger	atm	22.86
Tube diameter	m	0.0221
Ratio of tube length to tube diameter		579.19
Heat transfer coefficient in the coolant side (assumed const.)	$W/(m^2 \cdot K)$	13,500*

*The value of heat-transfer coefficient in the coolant side was calculated according to the geometry of a typical heat exchanger used in polyethylene reactor systems.

Table 4. Effects of Uncertainties of Physical and Transport Property Estimation on the Performance of the Heat Exchanger

Properties	Quantities	Heat Removed /Tube	Temp. Drop $(T_{in}^{V} - T_{out}^{V})$	Condens.
Base Case		**29.253 kJ/s**	**47.48 K**	**13.466 wt. %**
Deviations from Base Case				
Density	$\rho^V \times (100-3)\%$	−0.349%	−0.07	−0.628%
	$\rho^V \times (100+3)\%$	+0.297%	+0.06	+0.540%
	$\rho^L \times (100-5)\%$	+0.181%	+0.06	+0.251%
	$\rho^L \times (100+5)\%$	−0.168%	−0.06	−0.234%
Thermal conductivity	$\lambda^V \times (100-8)\%$	−1.039%	−0.69	−1.614%
	$\lambda^V \times (100+8)\%$	+1.080%	+0.60	+1.456%
	$\lambda^L \times (100-15)\%$	−0.786%	−0.26	−1.124%
	$\lambda^L \times (100+15)\%$	+0.577%	+0.18	+0.798%
Viscosity	$\eta^V \times (100-9)\%$	+1.477%	+0.61	+2.280%
	$\eta^V \times (100+9)\%$	−1.207%	−0.57	−2.142%
	$\eta^L \times (100-15)\%$	+0.362%	+0.12	+0.512%
	$\eta^L \times (100+15)\%$	−0.267%	−0.09	−0.392%
Heat capacity of vapor	$c_P^V \times (100-3)\%$	−1.190%	−0.23	−1.500%
	$c_P^V \times (100+3)\%$	+1.316%	+0.25	+1.590%
Diffusion coefficient	$D_{ij} \times (100-4)\%$	+0.304%	+0.04	+0.587%
	$D_{ij} \times (100+4)\%$	−0.287%	−0.03	−0.597%

There are two other properties—K values and partial enthalpies of vaporization—that were not included in Table 4, because they are phase-equilibrium-related properties and are quite different from typical volumetric, energetic, or transport properties of fluids of known composition. In this case, we are interested in the partial properties of the individual components that constitute the mixture. To find partial properties, one must differentiate data with respect to composition. Whenever experimental data are differentiated, there is a loss of accuracy. Therefore reliable experimental data related to phase-equilibrium properties are difficult to obtain, and the sizes of possible estimation errors are hard to know. It is not surprising that phase-equilibrium-related calculations are less accurate than other properties. For K values and partial enthalpies of vaporization, it is appropriate to perform sensitivity analyses based on predictions made using different estimation techniques.

Table 5 gives a detailed description of the methods for calculating K values and differential enthalpies of vaporization. Methods for calculating K values can be divided into two categories according to the two major forms of equations —Eqs. 7 and 9—in Table 5. The first of these two categories

Table 5. Estimation Methods for K Values and Partial Molar Enthalpy of Vaporization

Quantities		γ_i	Φ^0_{iL}	Φ_{iV}	Φ_{iL}
Using an equation of state					
$K_i = \dfrac{\phi_{iL}}{\phi_{iV}}$	(7)			Soave equation	Soave equation
$\Delta h_i = -RT\left(\dfrac{\partial \ln \phi_{iV}}{\partial T}\right)_{P,y} + RT\left(\dfrac{\partial \phi_{iL}}{\partial T}\right)_{P,x}$	(8)				
Using the Chao–Seader correlation					
$K_i = \dfrac{\gamma_i \phi^0_{iL}}{\phi_{iV}}$	(9)	Regular solution theory	Chao–Seader correlation	Redlich–Kwong equation	
$\Delta h_i = -RT\left(\dfrac{\partial \ln \phi_{iV}}{\partial T}\right)_{P,y} + RT\left(\dfrac{\partial (\gamma_i \phi^0_{iL})}{\partial T}\right)_{P,x}$	(10)				

uses an equation of state applicable to both liquid and vapor phases to calculate the fugacity coefficients for each component in the two phases. The methods in this category differ from each other according to the equations of state. In the second category, an activity coefficient γ_i in the liquid phase, a pure liquid fugacity coefficient Φ^0_{iL}, and a fugacity coefficient Φ_{iV} in the vapor phase are used to carry out out the calculations. In this case, different combinations of methods for evaluating γ_i, Φ^0_{iL}, and Φ_{iV} result in various ways of estimating K values. The widely applied Chao–Seader method is one such combination. Estimation techniques for the differential enthalpy of vaporization for each component follow directly the same methods of calculating Φ_{iV}, Φ_{iL}, γ_i, and Φ^0_{iL}, as shown by Eqs. 8 and 10. A detailed comparison of different methods for calculating K_i, made by Daubert et al. (1979), indicated that, overall, the Soave equation and Peng–Robinson equation are generally more successful than other methods.

If Eq. 9 is used to evaluate K values, the activity coefficient γ_i is commonly approximated by assuming that γ_i is independent of pressure at constant composition and temperature (Reid et al., 1987, 338), which is sensible at low or modest pressures. However at higher pressures, the effect of pressure on liquid-phase properties can be significant, and such an assumption is questionable. Moreover, in this case, there are several supercritical components, such as hydrogen and nitrogen. Estimation of pure liquid fugacity coefficients, Φ^0_{iL}, involves pure liquid molar volume calculations. For a supercritical component, its pure liquid at system temperature and pressure is hypothetical, hence the accuracy of pure liquid molar volume estimation is unclear. Using an equation of state applicable to both phases' K values can be calculated conveniently, however, especially for systems at high pressures and involving supercritical components. Knapp et al. (1982) performed a comprehensive review of the calculation of K values using equations of state. They considered four equations of state including Soave's modification of the Redlich–Kwong equation and the Peng–Robinson equation, and found that it is not possible to conclude that of the four equations, one particular equation is distinctly superior to the others.

Based on the preceding discussion, the Soave equation is employed in our model predictions. The set of model-prediction results referred to as the base case (method 1 in Table 6) was actually obtained using the Soave equation of state to evaluate both the K values and the differential heats of vaporization. The Chao–Seader correlation is the most preferred method in the second category because it is very useful in handling the problem of supercriticality. Hence, model sensitivities to uncertainties in phase-equilibrium-related properties were analyzed by comparing the results obtained by method 1 in Table 6 (the base case) with those by methods

Table 6. Effect of Different Methods on the Prediction of K Values and Partial Molar Enthalpy of Vaporization

		Method 1	Method 2	Method 3	Method 4	Method 5
Methods		Equation of State K_i by Eq. 7 Δh_i by Eq. 8	K_i by Eq. 7 Δh_i by Eq. 10 (Dev. from Method 1)	Chao–Seader Correlation K_i by Eq. 9 Δh_i by Eq. 10 (Dev. from Method 1)	K_i by Eq. 9 Δh_i by Eq. 8 (Dev. from Method 1)	Peng–Robinson Eq. K_i by Eq. 7 Δh_i by Eq. 8 (Dev. from Method 1)
Heat removed/tube		29.253 kJ/s	−0.280%	+25.238%	+31.238%	−1.605%
Temperature drop		47.48 K	−0.08 K	+1.37 K	+3.28 K	−0.21 K
Condensation		13.466 wt. %	−0.312%	+83.299%	+89.254%	−3.371%
	Inlet Mode Fraction	Outlet Mole Fraction in the Liquid Phase				
2-Methylpentane	0.036801	0.4042	0.4046	0.2357	0.2328	0.4032
Isopentane	0.006394	0.0414	0.0414	0.0295	0.0296	0.0412
n-Butene	0.12193	0.3833	0.3830	0.3435	0.3475	0.3822
Ethane	0.042039	0.0218	0.0218	0.0244	0.0246	0.0220
Ethylene	0.346206	0.1307	0.1307	0.1588	0.1600	0.1320
Nitrogen	0.162852	0.0088	0.0088	0.2039	0.2014	0.0091
Hydrogen	0.262476	0.0086	0.0086	0.0027	0.0026	0.0093

2–5 (corresponding to four different combinations of Eqs. 7 to 10). It can be seen that for method 2, where K_i values are calculated by using the Soave equation (Eq. 7), but Δh_i values are estimated by the Chao–Seader correlation (Eq. 10), the three major quantities differ only slightly from those in the base case (method 1). There are also small differences in the outlet liquid phase composition compared to the results in the base case. If both K_i and Δh_i are evaluated by the Chao–Seader correlation (method 3), the total condensation rate is increased by as much as 83% and the heat-removal rate is increased by 25%; however, the temperature drop is only increased by about 1.37 K. The resulting compositions in the outlet liquid phase are substantially different from the first two cases, in which K values are calculated by the Soave equation. One of the extraordinary results found here is that the outlet mole fraction of nitrogen in the liquid phase is as high as 20.39%, even higher than its mole fraction in the entering vapor mixture. This is obviously not reasonable for a sparingly soluble gas like nitrogen. This result supports the conclusion that equations of state are more successful than other methods for calculating K values for a system containing supercritical components at high pressures. The presence of nitrogen in this system is probably one cause of unsuccessful predictions by the Chao–Seader correlation. If we look at method 4, where K_i values are calculated by the Chao–Seader correlation, while Δh_i are estimated by the Soave equation, similar results are obtained as with method 3. This is not surprising because in both methods 3 and 4, K values are calculated using the Chao–Seader correlation. If as expected, both K_i and Δh_i are calculated using the Peng–Robinson equation of state (method 5), the results are very close to those obtained using the Soave equation (method 1). In summary, simulation results indicate that the model predictions are sensitive to the methods used for calculating K values, but are not as sensitive to the methods for estimating partial enthalpies of vaporization.

In conclusion, among all the physical and transport properties used in the model equations, K values are the main properties whose estimation accuracy significantly affects the model predictions. When gas-phase fluidized-bed polyethylene reactors are operated in condensed mode, the recycle stream is usually condensed at high pressure with the presence of some supercritical components at the operating temperature. It can be seen that an equation of state applicable to both the liquid and vapor phases gives better predictions of K values than the Chao–Seader correlation. Both Table 4 and Table 6 show that related to physical and transport property estimation errors, the model predictions differ by less than 0.70 K for temperature, less than 3.4% for condensation rate, and less than 1.7% for heat removal rate, if K values are calculated by two different equations of state applicable to both the liquid and vapor phases.

Model sensitivities to section length and convergence criteria

As described by Jiang et al. (1997), the set of differential material and energy balance equations can be converted to algebraic equations using finite difference approximations. When solving the model equations, the heat exchanger is divided into a number of sections. In each section, the set of resulting algebraic equations is solved by Newton's method combined with a globally convergent strategy. The physical and transport properties in the set of algebraic equations can be estimated using the values of mole fractions and temperatures: (1) at the beginning of each section, (2) at the end of each section, or (3) using the arithmetic average of mole fractions and temperatures at the beginning and at the end of each section. Taylor et al. (1986) found that for a given choice of section length, all three methods yield quite similar predictions of the total amount condensed and of the heat removed, while using the arithmetic average values predicts fairly accurately the composition and the temperature of the exit stream if noncondensable or sparingly soluble gases are present. Thus, in all the simulations of this work, the average values of the mole fractions and temperatures at the beginning and at the end of each section are used to estimate physical and transport properties within the section.

The cost of computation depends directly on the step size. Using a large section length, the number of times that the model equations must be solved decreases, leading to a reduction in computational time. However, large section lengths can cause a loss in simulation accuracy. Therefore, determining an acceptable size of length increment is necessary. Taylor et al. (1986) found that condenser design or simulation calculations can be satisfactorily carried out with length increments in the range of 25–50 cm. The choice of section lengths for satisfactory simulations will be discussed based on the available industrial data. Since most significant changes are expected at the beginning of condensation, simulation accuracy could strongly depend on the place where condensation starts and the step size in sections around that location. A trial-and-error method is actually used to make sure condensation starts as early as possible. Smaller section lengths are employed during the early stages of condensation to avoid inaccurate calculations. Another reason for choosing smaller section lengths is that convergence problems are most severe in the sections closest to the beginning of condensation. Therefore, no matter what step size is chosen in the following discussion, the section length at the start of condensation (4 or 5 sections) is always about 5–10 cm and is smaller than in the remaining part of the exchanger.

Choosing different section lengths, the corresponding computational times and the values of major quantities were obtained and are listed in Table 7. Comparing the results obtained by using step sizes of 12.80 cm and 102.44 cm for an exchanger with an overall length of more than 10 m, it can be seen that the relative discrepancy in the predictions of the condensation rate is 1.21%, which is less than the maximum uncertainty 3.37% relative to K value estimations. Therefore, length increments in the 25–50-cm range appear to be quite acceptable section lengths for simulations of this industrial heat exchanger.

A second concern is convergence toward the solution. For a set of nonlinear equations of the form:

$$F(X) = 0, \tag{11}$$

using Newton's method combined with a globally convergent strategy, the new step is

$$X_{\text{new}} = X_{\text{old}} + \theta \delta X, \tag{12}$$

Table 7. Model Sensitivities to Step Size and Convergence Criterion

Section Length, cm	Comput. Time, s	Heat Removed/ Tube, kJ/s	Temp. Drop, K	Condens. wt. %
102.4	149.6	28.979	47.20	13.318
51.2	247.1	29.169	47.40	13.418
25.6	**306.7**	**29.253**	**47.48**	**13.466**
12.8	695.9	29.290	47.51	13.481

Convergence Criterion	Comput. Time, s	Heat Removed/ Tube, kJ/s	Temp. Drop, K	Condens. wt. %
$\sqrt{\sum_{i=1}^{n} F_i^2} < 2.0$	**306.7**	**29.253**	**47.48**	**13.466**
$\sqrt{\sum_{i=1}^{n} F_i^2} < 2.0\times10^{-1}$	594.6	29.273	47.48	13.463
$\sqrt{\sum_{i=1}^{n} F_i^2} < 2.0\times10^{-2}$	639.6	29.273	47.49	13.463
$\sqrt{\sum_{i=1}^{n} F_i^2} < 2.0\times10^{-3}$	597.4	29.273	47.49	13.463

where

$$\delta X = -[J]^{-1}(F) \tag{13}$$

and θ is a parameter with values in the range of $0.0 < \theta \leq 1.0$. For the systems we are investigating the typical unscaled values of the discrepancy function F_i can vary from the magnitude of 10^{-3} to 10^{+5}, and the resulting Jacobian matrix $[J]$ could be ill-conditioned, leading to very slow convergence or no convergence at all. The unscaled values of unknowns, X_i, also range from the magnitude of 10^{-3} to 10^{+3}. To reduce convergence problems, the values of both the unknown variable X_i and discrepancy function F_i were scaled so that their typical values were all of order unity. It was found that there were still some convergence difficulties when solving the set of nonlinear equations in some sections along the length of the heat exchanger, especially if the convergence criterion was very small. The reason is that it is difficult to achieve the same convergence criterion for equations representing mass and heat transfer. The heat-transfer equations tend to converge 10^2 times more slowly than mass-transfer equations. In globally convergent methods, a searching process is involved to find a θ so that $f(X_{old} + \theta\delta X)$ has decreased sufficiently, where f is defined by

$$f = F \cdot F/2. \tag{14}$$

That means that even for a relatively large convergence criterion, the actual values of f could be very much smaller than the convergence criterion because there is a continuing searching process to minimize f for each new step. In fact, when solving the model equations, f is of order 10^{-4} in most sections, with only several exceptions, even if the overall convergence criterion is as large as 2.0. On the other hand, the magnitude of temperature is much greater than other mass and composition variables in the unknown variables, but it is not necessary to have the same calculation accuracy for temperatures, because there is no necessity for temperature predictions as accurate as 0.001 K in industrial simulations.

The sensitivities of model predictions to the choice of convergence criteria were performed and the results are shown in Table 7. It can be seen that for convergence criteria ranging from 2.0 to 2.0×10^{-3} the condensation rate and temperature are almost unaffected, as expected, and the relative discrepancy is less than 0.7% between the predictions of the heat removal rate. It should be noted that no matter what overall convergence criterion was chosen, the model equations converged within 10^{-3} in most cases, with only several occasions near the convergence criteria shown in Table 7. For different convergence criteria, therefore, different step sizes are selected; these different step sizes also account for different computer times and simulation results.

From the preceding analysis, it can be seen that, if the model equations are solved using Newton's method combined with the globally convergent strategy, choosing a convergence criterion as high as 2.0 does not significantly influence simulation results compared to the results obtained using a convergence criterion of 2.0×10^{-3}.

Effects of Operating Conditions on the Heat-Removal Rate

In the previous two sections, good agreements have been obtained between the model simulation results and the industrial operating data. The results of model sensitivity analysis have indicated that if K values are estimated using an equation of state applicable to both the liquid and vapor phases, the model predictions are not sensitive to the uncertainties related to physical and transport property estimations. It has also been demonstrated that appropriate step-size and convergence criteria were selected when solving the model equations. Based on these results, one can now use the model to investigate the effect of operating conditions on heat removal from the reactor, especially the effect of noncondensable gases on condensation heat transfer.

The final result of the heat-removal rate for a particular amount of recycled stream depends on the joint operating conditions of the heat exchanger and reactor system. In order to have a better understanding of how different operating conditions affect heat removal, the effects of individual factors were investigated first. Changing only one operating variable at a time and keeping all the other conditions unchanged, the resulting major quantities representing the performance of the heat exchanger were compared to the base case (see Table 8). The four operating conditions chosen here are the conditions most commonly adjusted without changing the catalyst system or the process equipment in industry.

To further increase heat removal, Jenkins et al. (1986) suggested that the dew point of the recycle stream be increased by adding a condensable fluid, which is inert to the catalyst, reactants, and the products of the polymerization reaction, to the recycle stream. Examples of suitable inert condensable fluids may be selected from saturated hydrocarbons containing from 2 to 8 carbon atoms, such as n-pentane, isopentane, n-hexane, and isohexane. Isohexane was chosen for this simulation study. In the recycle gas mixture, both H_2 and N_2 are

Table 8. Effects of Individual Factors on the Performance of the Heat Exchanger

Quantities	Heat Removed /Tube	Temp. Drop $\Delta T = T_{in}^V - T_{out}^V$	Condens.
Base case	**29.253 kJ/s**	**47.48 K**	**5.692 mol %**
	Deviation from Base Case		
36.84 mol % of N_2 replaced by C_6H_{14}	+68.88%	+0.65	+183.33%
6.14 mol % of C_6H_{14} replaced by N_2	−16.00%	−0.60	−37.36%
Inlet cooling water T −16.55 K	+51.43%	+15.16	+69.35%
Inlet cooling water T +17.46 K	−50.47%	−15.21	−73.94%
Inlet gas flow rate +30.00 wt. %	−7.70%	−3.20	−14.04%
Inlet gas flow rate −30.00 wt. %	+6.80%	+2.72	+13.40%
Cooling-water flow rate +55.90 wt. %	+5.72%	+2.35	+11.21%
Cooling-water flow rate −37.35 wt. %	−9.99%	−4.24	−18.94%

noncondensable gases, but H_2 is used as a polymerization chain transfer agent, and no change can be made to its level without affecting product quality. However, N_2 is merely an inert gas used to carry the catalyst into the reactor, and therefore might be replaced by a fluid like C_6H_{14} (isohexane). If the compositions of other components remain unchanged, replacing 36.84% of the original N_2 by an equal number of moles of C_6H_{14}, the heat-removal rate is increased by 68.88%, the exiting vapor temperature is 0.65 K lower than before (the entering vapor temperature T_{in}^V is fixed in all the cases), and total mole percentage condensed is increased by 183.33%. Replacing 36.84% of N_2 by C_6H_{14} makes the recycle gas mixture condense right at the inlet of the heat exchanger. This is the highest level that could be tolerated in the reactor system. If some of the condensable gas, C_6H_{14}, is replaced by noncondensable N_2 to increase the mole fraction of N_2 by 6.14%, both the heat-removal rate and total mole percentage condensed are decreased substantially. The reason that N_2 was not increased by as much as 36.84% is that the recycle gas mixture will not condense at all under these conditions.

If the entering cooling-water temperature is reduced by 16.55 K, the heat-removal rate is increased by 51.43%, the level of condensation is increased by 69.35%, and the outlet vapor temperature is decreased significantly, to 15.16 K lower than in the base case. Thus, in this case, heat removed is increased by both the greater temperature difference and the higher level of condensation. When replacing noncondensable gas by a condensable material, however, the heat-removal rate is increased mainly due to the higher level of condensation. Looking at the changes in the major quantities from increasing the recycle gas flow rate, it can be seen that raising the inlet gas flow rate by 30.00%, the heat-removal rate is not reduced as significantly as in the first two cases. If the cooling-water flow rate is increased by 55.90%, the heat-removal rate only increases by 5.72%. On the other hand, the heat-removal rate is only decreased by 10% if the cooling-water flow rate is reduced by 37.35%. This one-factor-at-a-time testing indicates that the concentration of noncondensable gas and entering-cooling-water temperature are two variables that substantially influence the heat removal from the reactor. However, changing the cooling-water flow rate does not have a large effect on the heat-removal rate. From the point of view of industrial practice, reducing cooling-water temperature may not be possible without significantly increasing operating or capital costs. Replacing a portion of the N_2 by a suitable inert condensable fluid may be a much more convenient option.

With the cooling-water flow rate held constant, a complete three-factor–two-level factorial simulation experiment was carried out to investigate any possible joint influences of more than one factor on the performance of the heat exchanger and reactor system. It was shown that two-factor interactions and three-factor interactions are not significant (Jiang, 1997).

Discussion and Conclusions

Using the one-dimensional nonequilibrium model for the multicomponent condensation described by Jiang et al. (1997), a vertical heat exchanger in an industrial polyethylene reactor system has been simulated at industrial conditions corresponding to ethylene homopolymerization, and copolymerization of both ethylene/butene and ethylene/hexene. The sensitivities of model predictions to the uncertainties in physical and transport property estimations and to the choices of step size and convergence criterion were analyzed. The effects of operating conditions on the rate of heat removal from the reactor were investigated, leading to the following conclusions:

1. Reasonable results and good agreement between simulation results and industrial measurements have been obtained when simulating multicomponent condensation in a vertical heat exchanger in an industrial polyethylene reactor system. Starting our calculation from the top of the heat exchanger, it was found that the model can predict the outlet temperature of the vapor mixture T_{out}^V and the entering cooling water temperature T_{in}^c within an accuracy of ± 5 K for an approximate 50 K difference between inlet gas temperature T_{in}^V and outlet vapor phase temperature T_{out}^V.

2. Except for K values, the model predictions are not particularly sensitive to the expected uncertainties associated with all the other physical and transport property estimations. In industrial polyethylene reactor systems, the recycle gas stream is condensed at high pressure. Under the operating temperatures of the heat exchanger, supercritical components are involved in the recycle gas mixture. Therefore, it is recommended that an equation of state applicable to both the liquid and vapor phases be utilized to calculate the K values. Using two different equations of state to calculate the K values, the differences in model predictions were less than 0.70 K in temperature predictions, less than 3.4% in condensation rate predictions, and less than 1.7% in heat-removal rate predictions.

3. Model simulations quantitatively demonstrate why, and how severely, noncondensable gases impede condensation heat transfer. Replacing a portion of noncondensable gas N_2 with a condensable fluid can substantially increase the heat removal using the latent heat of vaporization, since both the

gas and the fluid are inert to polymerization reactions. Reducing the cooling-water temperature is also an effective way of enhancing heat transfer.

Acknowledgment

The authors thank Queen's University, the School of Graduate Studies and Research, and the Natural Science and Engineering Research Council of Canada for support of this research.

Notation

A = interfacial area, m^2
A_{outs} = the surface area of the tube outside, m^2
D_{ij} = Fickian diffusivity for binary mixture, $m^2 \cdot s^{-1}$
(F) = vector of dependent functions
K_i = vapor/liquid equilibrium constants
m_V = total molar flow rate of the vapor mixture, $kmol \cdot s^{-1}$
m_c = coolant mass flow rate, $kg \cdot s^{-1}$
x = mole fraction in liquid phase
X = vector of independent variables
y = mole fraction in vapor phase
η = viscosity, $Pa \cdot s$
λ = thermal conductivity, $W \cdot m^{-2} \cdot K^{-1}$
ρ = density, $kg \cdot m^{-3}$

Literature Cited

Burdett, I. D., "The Union Carbide UNIPOL Process: Polymerization of Olefins in a Gas-Phase Fluidized Bed," AIChE Meeting, Washington, DC (1988).

Butterworth, D., *Heat Exchanger Design Handbook*, E. U. Schlünder, ed., Hemisphere, Washington, DC, p. 2.6.2 (1983).

Choi, K. Y., and W. H. Ray, "Recent Developments in Transition Metal Catalyzed Olefin Polymerization—A Survey: I. Ethylene Polymerization," *J. Macromol. Sci. Rev. Macromol. Chem. Phys.*, **C25**(1), 1 (1985).

Daubert, T. E., M. S. Graboski, and R. P. Danner, Documentation of the Basis for Selection of the Contents of Chapter 8—Vapour-Liquid Equilibrium K-Values in Technical Data Book—Petroleum Refining, No. 8-78, Amer. Petrol. Inst., Washington, DC (1979).

DeChellis, M. L., and J. R. Griffin, "Process for Polymerizing Monomers in Fluidized Beds," U.S. Patent No. 5,352,749 (Oct. 4, 1994).

DeChellis, M. L., J. R. Griffin, and M. E. Muhle, "Process for Polymerizing Monomers in Fluidized Beds," U.S. Patent, 5,405,922 (Apr. 11, 1995).

Jenkins, J. M., III, R. L. Jones, T. M. Jones, and S. Beret, "Method for Fluidized Bed Polymerization," U.S. Patent, 4,588,790 (May 13, 1986).

Jiang, Y., "Nonequilibrium Modeling of Multicomponent Condensation in a Vertical Heat Exchanger of a Polyethylene Reactor," PhD Thesis, Queen's Univ., Kingston, Ont., Canada (1997).

Jiang, Y., K. B. McAuley, and C. C. Hsu, "Nonequilibrium Modeling of Condensed Mode Cooling of Polyethylene Reactors," *AIChE J.*, **43**(1), 13 (1997).

Knapp, H., R. Döring, L. Oellrich, Y. Plöcker, and J. M. Prausnitz, *Chemistry Data Series*, Vol. VI, *VLE for Mixtures of Low Boiling Substances*, D. Behrens and R. Eckerman, eds., DECHEMA, Frankfurt A.M., Germany (1982).

Reid, R. C., J. Prausnitz, and B. E. Poling, *The Properties of Gases and Liquid*, McGraw-Hill, Toronto (1987).

Rosson, H. F., and J. A. Meyers, "Point Values of Condensing Film Coefficients Inside a Horizontal Tube," *Chem. Eng. Prog. Symp. Ser.*, **61**(59), 190 (1965).

Taylor, R., R. Krishnamurthy, and J. S. Furno, "Condensation of Vapour Mixtures: 1. Nonequilibrium Models and Design Procedures," *Ind. Eng. Chem. Process Des. Dec.*, **25**, 83 (1986).

Manuscript received July 3, 1996, and revision received Apr. 4, 1997.